Porous Chitosan Microspheres as Microcarriers for 3D Cell Culture

Lixia Huang,[1‡] *Lin Xiao,*[1‡] *Abishek Jung Poudel,*[1] *Jixiang Li,*[2] *Ping Zhou,*[3] *Mario Gauthier,*[4] *Haiqing Liu,*[2*] *Zhihong Wu,*[5*] *Guang Yang*[1*]

[1] Department of Biomedical Engineering, College of Life Science and Technology, Huazhong University of Science and Technology, 1037 Luoyu Road, Wuhan 430074, China.

[2] Fujian Provincial Key Laboratory of Polymer Materials, College of Material Science and Engineering, Fujian Normal University, 8 Shangsan Road, Fuzhou 350007, China.

[3] Institute of Organ Transplantation, Tongji Medical School, Huazhong University of Science and Technology, 13 Hangkong Road, Wuhan 430074, China.

[4] Department of Chemistry, University of Waterloo, 200 University Avenue West, Waterloo N2L 3G1, Canada.

[5] Department of Orthopaedic Surgery, Peking Union Medical College Hospital, Peking Union Medical College, 1 Shuaifuyuan Road, Beijing 100730, China.

Corresponding Authors

*E-mail: yang_sunny@yahoo.com. Tel: +86 27-87793523. Fax: +86 27-87792265.

*E-mail: haiqing.liu@gmail.com. Tel: +86 591-83404938. Fax: +86 591-83404938.

*E-mail: wuzh3000@126.com. Tel: +86 10-69154259. Fax: +86 10-69154259.

‡These authors contributed equally.

ABSTRACT: Highly porous chitosan microspheres (CSM) were prepared through emulsion-based thermally induced phase separation (TIPS) without using toxic crosslinkers and chemical porogenic agents other than ice. The CSM had an average diameter of ~150 μm with interconnected pores varying from 20~50 μm in size. Due to their excellent biocompatibility and unique porous structure, high-performance hepatocyte culture in three-dimensional (3D) space was achieved using the CSM as microcarriers, as cell growth also took place within the internal pores of the CSM, besides their external surface, and multidirectional cell–cell interactions were observed. Enhanced cellular activity and functions were obtained with the CSM microcarriers as compared with 2D cell culture. It is believed that these CSM microcarriers provide a promising platform for 3D cell culture *in vitro*.

KEYWORDS: Chitosan, Porous microspheres, Microcarriers, 3D cell culture, Hepatocytes.

Graphical abstract:

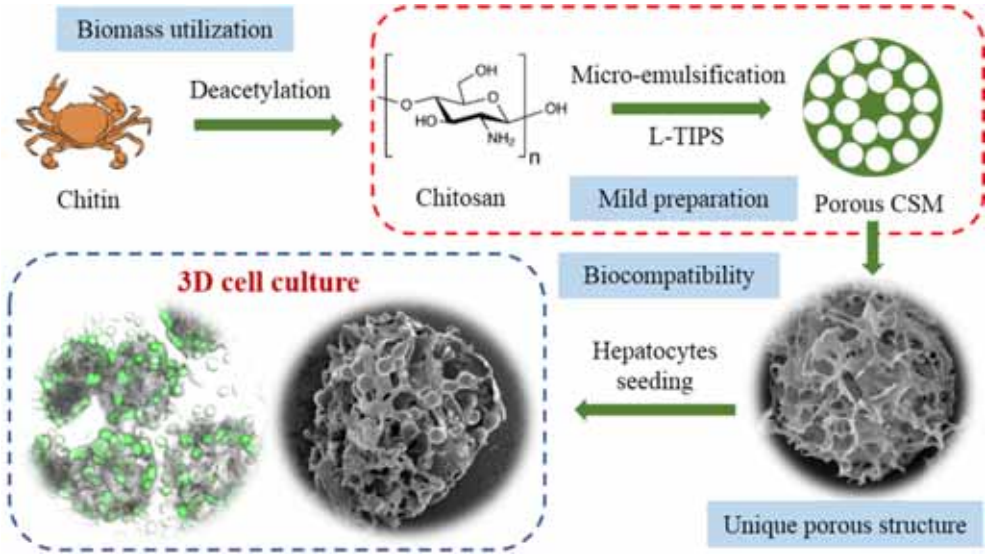

Highlights

- CSM were prepared by a mild procedure, free of toxic crosslinking agents and porogens.
- The CSM have excellent biocompatibility and a unique porous structure.
- Convincing evidence for 3D cell culture was obtained using the CSM as microcarriers.
- The CSM microcarriers are favorable to maintaining cellular activity and functions.

1. INTRODUCTION

Traditional cell plate culture has been questioned because of potential changes in morphology and gene expression, often resulting in distortions in cell behavior and biological functions of cultured cells as compared with cells in natural organisms and tissues (Asghar et al., 2015). To better maintain cell morphology, behavior and functions, the concept of three-dimensional (3D) cell culture was proposed, that is cell growth in a 3D environment with sufficient and multidirectional cell–cell interactions mimicking the *in vivo* architecture of natural organs and tissues (Achilli, Meyer, & Morgan, 2012; Pampaloni, Reynaud, & Stelzer, 2007). Natural polymer-based scaffolds have received broad attention for 3D cell culture due to their good biocompatibility and designed structure (Higuchi et al., 2014; Kehr, 2016; Mazza et al., 2015; Motealleh, Hermes, Jose & Kehr, 2018; Motealleh & Kehr, 2017; Song et al., 2017). For example, the group of Kehr developed alginate-based 3D hydrogel scaffolds containing periodic mesoporous organosilica or zeolite nanoparticles functionalized with the chiral biopolymers poly(L-lysine) and poly(D-lysine). Chirality-dependent cell adhesion and cell migration were investigated in these hydrogel scaffolds (Kehr, 2016; Motealleh et al., 2017; Motealleh et al., 2018).

The microcarrier culture technique, first introduced by van Wezel (1967), relies upon microspheres derived from various materials, with either a porous or a non-porous structure, as supports for anchoring cell lines. The main advantages of the microcarrier technology include a high surface area to mass ratio, the use of stirred microcarrier suspension culture, and easy scale-up making it possible to culture a wide range of animal cells in high yield (Chen, Reuveny, & Oh, 2013). A wide range of commercial and experimental microcarriers have emerged over the past few decades (Duan et al., 2015; Fang et al., 2014; Healthcare & Biosciences, 2005; Yu,

Kornmuller, Brown, Hoare, & Flynn, 2017). However, it should be noted that most of the existing microcarriers only enable cell attachment and growth on their outermost surface, or else on their external pore surface, with either no or only unidirectional cell–cell interactions. This is in essence very similar to monolayer cell culture in plates, and thus may not be considered 3D cell culture in the strict sense. Indeed, real 3D cell culture with microcarriers should enable cell growth within the microcarriers in addition to their surface, with sufficient and multidirectional cell–cell interactions, to mimic more closely the *in vivo* environment experienced by cells in natural organs and tissues (Achilli et al., 2012). This is considered crucial for the cells to present normal behavior and function. Chung et al. (2008) fabricated amine-functionalized microcarriers with a well-interconnected pore structure from poly(lactic-*co*-glycolic acid) (PLGA), through gas-promoted foaming in a water-in-oil-in-water double emulsion, for cell cultivation and injectable delivery. Unfortunately, the seeded cells barely infiltrated the inner pores of these supports but rather attached onto their outer surface for the most part. The authors hypothesized that the highly porous skeletal structure of the microcarriers likely did not provide sufficient anchoring surface area for cell attachment within the interior void spaces. Many other microcarriers were reported that only achieved cell growth on their outer surface (Duan et al., 2015; Yu et al., 2017; Zhang et al., 2018). More recently, Yan et al. (2018) reported porous microcarriers fabricated from strontium-substituted hydroxyapatite-*graft*-poly(γ-benzyl L-glutamate) nanocomposites. The adhesion and infiltration of rabbit adipose-derived stem cells (ADSCs) within the internal cavities of these microcarriers were confirmed by confocal microscopy. It was shown that labeled ADSCs could be detected at 1/8, 2/8, 3/8 and 4/8 diameter depths of the microcarriers, which implied that cell attachment and growth were allowed in the innermost regions of these microcarriers.

106 The biopolymer chitosan, obtained by the deacetylation of chitin, has been widely applied in
107 the biomedical field because of its non-toxicity and good biodegradability (Anitha et al., 2014;
108 Pellá et al., 2018). Different chitosan-based porous macroscopic scaffolds were developed for 3D
109 cell culture (Tripathi & Melo, 2015; Westin, Trinca, Zuliani, Coimbra & Moraes, 2017). As an
110 example, Tripathi et al. (2015) synthesized sponge-like composite agarose–chitosan scaffolds in
111 various forms including monolith and disc shapes. Primary hepatocyte growth and cell–cell
112 interactions within the interconnected pore network of these scaffolds were observed. Chitosan-
113 based microcarriers were also reported for cell culture (Custódio, Cerqueira, Marques, Reis &
114 Mano, 2015; Tedesco et al., 2018; Wu et al., 2011; Zhang et al., 2018). For example, Zhang et al.
115 (2018) developed chitosan-based microcarriers reinforced with graphene oxide through an acid-
116 dissolution/alkali-precipitation approach. These hybrid microspheres were able to support stem
117 cell expansion, growth and proliferation. Custódio et al. (2015) also developed chitosan
118 microcarriers, bioconjugated on their surface with monoclonal antibodies favoring cell capture
119 and subsequent cell expansion. Although multiple chitosan-based microcarriers have been
120 investigated over the past decade, there is only one report, by Fang et al. (2014), for which 3D
121 cell culture was supported in the true sense, enabling cell migration to the inside of the carrier
122 and multidirectional cellular interactions. This may be because porous chitosan microspheres are
123 usually prepared by crosslinking emulsions, i.e. chitosan emulsion droplets are first formed, and
124 then stabilized with a crosslinking reagent such as glutaraldehyde. Unfortunately, the pores of
125 chitosan microspheres obtained by that method are not large enough to accommodate cells (Wu
126 et al., 2011). Fang et al. (2014) first prepared porous chitosan microspheres with large pores
127 (47.5 ± 5.4 μm) by a phase separation technique. Microcarriers, named PEC, were then
128 fabricated by coating the chitosan microspheres with poly(L-glutamic acid) *via* electrostatic

interaction and evaluated for cartilage regeneration. The authors confirmed that the poly(L-glutamic acid)-coated PEC microcarriers enabled the proliferation potential of chondrocytes, with cell infiltration and survival in the inner regions of the microcarriers. However they also stated that the poly(L-glutamic acid) modification played a vital role in 3D cell culture, as it enhanced the hydrophilicity of the microcarriers. We previously reported a simple and reliable emulsion-based thermally induced phase separation (TIPS) procedure to fabricate chitosan microspheres with large pores (J. Li et al., 2017). By adapting this preparation method for the current investigation, chitosan microspheres (CSM) with superior biocompatibility and a highly porous structure were obtained and fully characterized. In particular, the suitability of these as-prepared chitosan microspheres as microcarriers for 3D hepatocyte culture was confirmed, without requiring surface modification.

2. Materials and Methods

2.1. Materials and cell line.

Chitosan (degree of deacetylation > 95%) was obtained from Sigma-Aldrich. Its viscosity-average molecular weight, determined with an Ubbelohde viscometer at 25°C and the Mark-Houwink-Sakurada equation $[\eta] = KM^{\alpha}$, where $K = 1.8\times10^{-6}$ and $\alpha = 0.93$ (Costa, Teixeira, Delpech, Souza, & Costa, 2015), was $M_v = 1.02\times10^{6}$. The surfactants Span 80 (S80) and Tween 60 (T60), acetic acid, petroleum ether and sodium hydroxide (NaOH) were purchased from Shanghai Sinopharm Chemical Reagent Co. Ltd. All the reagents were analytical grade and were used without further purification.

A human fetal hepatocyte line, L-02, obtained from Tongji Medical School, Huazhong University of Science and Technology (Wuhan, China) was cultured in RPMI-1640 medium

with 10% fetal bovine serum and 1% antibiotics (100 mg/mL streptomycin and 100 U/mL penicillin), by incubation at 37°C in a humidified atmosphere containing 5% CO_2.

2.2. Preparation of porous chitosan microspheres (CSM).

To fabricate porous CSM appropriate as 3D culture supports for the L-02 cells, a combination of micro-emulsification and low temperature thermally induced phase separation (L-TIPS) techniques was selected and adapted from the procedure described in our previous work (J. Li et al., 2017). Specifically, a 1% (w/v) aqueous chitosan solution was prepared by dissolving chitosan powder into 1% (w/v) aqueous acetic acid solution (ca. 0.167 M), to serve as the dispersed phase. The continuous phase was petroleum ether containing S80 and T60 emulsifiers in a mass ratio (S80/T60) of 4.8/0.2, and a total mass content of 5% (w/v). The chitosan solution (10 mL) was added drop-wise into 50 mL of the continuous phase at 40°C under magnetic stirring at 1000 rpm to obtain a w/o emulsion. After stirring for 3 h, the emulsion was quenched and stored at -20°C for 3.5 h. A phase inversion liquid, in the form of 100 mL 1% (w/v) NaOH solution in ethanol and water (14:1, v/v), was then poured into the quenched emulsion under mild stirring. The chitosan microspheres that formed were collected by centrifugation and were successively washed with water and ethanol until the supernatant became neutral, before drying under vacuum at 30°C. The as-prepared CS microspheres are identified as CSM (Scheme 1).

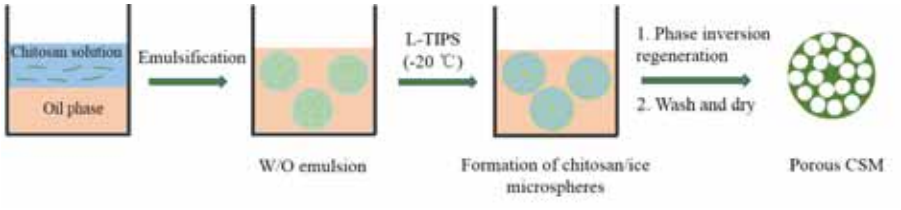

Scheme 1. Fabrication procedure for the porous chitosan microspheres (CSM).

2.3. Characterization of the CSM.

The morphology of the CSM was observed on a scanning electron microscope (SEM) (Quanta 200, FEI) at an accelerating voltage of 20.0 kV after sputter-coating with gold. To characterize the distribution of pores within the particles, the cross-sectional morphology of the CSM was visualized as follows. The CSM were first stained with 1% (w/v) Rhodamine B solution in ethanol. After vacuum drying at 30°C for 10 h, they were embedded in paraffin and cut into 5 μm thick slices on a microtome (Leica RM2235). The cross-section structure was then observed on an Olympus BX51 optical microscope. The specific surface area was characterized by nitrogen adsorption-desorption isotherm analysis at 77 K (Micromeritics ASAP 2020 apparatus). Other physical properties that were characterized include the porosity, pore size distribution, density, water absorption capacity and the elastic modulus. The protocols for these studies are provided in the Supplementary Information.

2.4. Biocompatibility assay.

The contact cytotoxicity and non-contact cytotoxicity of the CSM were evaluated with L-02 cells. Blood compatibility assays were also performed for the CSM through determination of the hemolysis rate. The specific protocols used for these studies are provided in the Supplementary Information.

2.5. Cell attachment on/in the CSM.

A CSM suspension in water (4 mg/mL), sterilized by autoclaving, was added to a L-02 cell suspension in culture medium (1×10^5 cells/mL) in a volume ratio of 1:1. After gentle mixing on a shaker for 1 h, the cell/CSM suspension was transferred to a 24-well plate at 1 mL/well. After incubation for 10 h the cells were washed with PBS three times, followed by progressive

dehydration in 30%, 50%, 70%, 90%, 95% and 100% ethanol for 10 min each. After freeze-drying, the samples were carefully removed with forceps and placed on conductive adhesive tape on a platform for SEM (SU8010, Hitachi) observation after sputter-coating with gold. The fractured surface of the CSM/cell complex was also obtained and imaged by SEM after the same pretreatment. To determine the cell distribution within the CSM, the cells were stained with Calcein-AM (2 μM) and observed by laser scanning confocal microscopy (Olympus FV1000, Japan) at different depths of the CSM after incubation for 48 h.

2.6. Cell activity evaluation.

The viability of cells cultured on the CSM microcarriers was assessed using a live/dead assay kit (Dojindo, Japan). The L-02 cells were cultured with 2 mg/mL of CSM in a 35 mm confocal dish (In Vitro Scientific, USA) for 12, 24, 48 or 72 h, respectively. Working solutions of Calcein-AM (2 μM) and PI (4 μM) were prepared from stock solutions. After washing the cells with PBS solution three times, an equimolar mixture of dyes was added at 500 μL/well. After incubation at 37°C for 30 min, the samples were observed by laser scanning confocal microscopy (Nikon A1, Japan) using an excitation wavelength of 490 nm and the green emission at 515 nm to observe the live cells, while an excitation wavelength of 535 nm and the red emission at 615 nm were used to observe the dead cells. To further evaluate cell activity, the cell shape was determined by laser scanning confocal microscopy (Olympus FV1000, Japan) after incubation with the CSM for 48 h. The cell nuclei and cell membranes were stained with Hoechst 33258 (Beyotime, China) (10 μg/mL) and DiI (Beyotime, China) (10 μM), respectively. An excitation wavelength of 405 nm and the blue emission were used to observe the cell nuclei, while an excitation wavelength of 559 nm and the red emission served to observe the cell membranes.

2.7. Albumin and urea secretion.

The concentration of albumin (ALB) and urea in the culture medium was determined by the competitive enzyme linked immunosorbent assay (ELISA). The cell culture supernatants were collected in a sterile tube after centrifugation for 20 min at 2000 rpm. Aliquots of standards and diluted supernatants (100 μL each) were added to the antibody-coated wells. After incubation for 1 h, the wells were washed three times and incubated with ALB antibody labeled with horseradish peroxidase (HRP) for 1 h. After washing three times, 3,3',5,5'-tetramethylbenzidine (TMB) substrate solution was added before incubation in the dark for 30 min. The OD values were measured spectrophotometrically at 450 nm. The concentration of ALB in the samples was determined by comparing the OD values for the samples to a standard curve.

2.8. Gene expression.

Total RNA extraction from the L-02 cells was achieved with a RNApure Tissue & Cell Kit (CWBIO, China), after the cells were cultured with 2 mg/mL of CSM for 48 h in a 6-well plate at a seeding density of 30×10^4 cells/well. The total RNA was adjusted to 1.0 μg/sample before it was transcribed into cDNA with a Frist Strand cDNA Synthesis Kit (TOYOBO, Japan) according to the instructions. Fluorescence-based quantitative PCR was conducted using a 7500 Fast Real-time PCR system (Applied Biosystems, USA) and SYBR Select Master Mix (Applied Biosystems, USA) according to the manufacturers' guidelines. The specific quantitative primers were synthesized by BGI (Shenzhen, China) with sequences as follows:

GAPDH: 5'- ACAACTTTGGTATCGTGGAAGG-3'(sense) and 5'-GCCATCACGCCACAGTTTC-3'(antisense);

CYP2E1: 5’-GGGAAACAGGGCAATGAGAG-3’(sense) and 5’-GGAAGGTGGGGTCGAAAGG-3’(antisense);

GST: 5’-AACCTCAACTGAACAGCATCC-3’(sense) and 5’-GGTTGGTCTTGGTCCTCCTAT-3’(antisense);

MRP: 5’-AAGGAGGTACTAGGTGGGCTT-3’(sense) and 5’-CCAGTAGGACCCTTCGAGC-3’(antisense);

ASS1: 5’-TCCGTGGTTCTGGCCTACA-3’(sense) and 5’-GGCTTCCTCGAAGTCTTCCTT-3’(antisense).

2.9. Proteomics analysis.

The cells were lysed and total protein extraction was achieved by the same treatment described above. The protein concentration was determined by the Bradford protein assay. Then the samples were thermally denatured, reduced and alkylated prior to trypsin (Progmega) digestion for 15 h. The digested proteins were labelled with an iTRAQ reagent kit (8 plex, Applied Biosystems) according to the protocol supplied. The fractionated peptide mixtures were analyzed on a Q-Exactive mass spectrometer equipped with an EASY-nLC 1000 System (Thermo Fisher Scientific). The parameters for the spray voltage, capillary temperature and declustering potential of the source ionization were set at 2.1 kV, 250°C and 100 V, respectively.

2.10. Western blot analysis.

For western blot analysis, equal amounts of proteins (20 μg/sample) were separated on SDS-PAGE and transferred onto a PVDF membrane. After blocking overnight, the membrane was successively incubated with primary antibody and HRP-conjugate secondary antibody at

37°C for 1 h with shaking. The bands were visualized using Pierce ECL Western Blotting (Thermo Scientific, USA).

2.11. Statistical analysis.

Quantitative data are expressed as the arithmetic mean value ± standard deviation (SD). All the quantitative results were obtained from at least triplicate samples. A t-test was used to detect differences between groups, with $p < 0.05$ considered statistically significant and $p < 0.001$ considered highly statistically significant.

3. RESULTS AND DISCUSSION

3.1. Morphological and physical properties of the CSM.

The structure of the CSM obtained by the method described is visible in Figure 1. The microspheres have a spherical topology, a diameter of ca. 150 μm and a large number of irregular pores varying from 20 to 50 μm in diameter (Figure 1A). The pores are interconnected, as can be seen more clearly from the enlarged image section provided in Figure 1B. This was further confirmed by optical microscopy of the microtomed material providing cross-section views of the CSM as exemplified in Figure 1C, likewise revealing the presence of multiple interconnected pores in the 20~50 μm range throughout the whole particles. It was demonstrated in our previous study (J. Li et al., 2017) that such a structure is due to the mechanism of TIPS. Upon quenching the emulsion droplets to -20°C, solid–liquid phase separation occurs within them, and the water/acetic acid solvent mixture undergoes slow crystallization allowing the ice crystals to gradually grow larger, leaving behind irregular pores on and within the CSM after the ice crystals are removed. It was further verified that the pore size in the microspheres could be controlled by adjusting the quenching temperature (Fang et al., 2014; J. Li et al., 2017): The pore

size decreases as the quenching temperature is lowered, because a relatively fast crystallization process produces smaller crystals. TIPS is a well-established method for the preparation of porous materials. Crystalline polymers such as polylactide (PLA) and PLGA are often employed to prepare porous materials by the TIPS technique (Ahmadi, Mordan, Forbes, & Day, 2011; Nina, Raheleh, & M., 2015; Zhang & Ma, 2015), but chitosan-based porous materials have been also obtained by the same approach (J. Li et al., 2017; Tripathi et al., 2015).

The porosity of the CSM, determined by a liquid displacement method, was as high as 98.0±0.5 %, which leads to a very low density of 0.040±0.006 g/cm^3 for the dry CSM. The distribution of pore sizes was also estimated by mercury injection. The results in Figure 1D demonstrate that most pores are within a range of 10~60 μm, with an average diameter of 27.8 μm, which is in good agreement with the SEM observations. The specific surface area was measured to be 30.0±0.7 m^2/g, much higher than for the commercial Cytopore microcarriers (reported to be 1.0~3.0 m^2/g) (Healthcare & Biosciences, 2005; Ikonomou, Drugmand, Bastin, Schneider, & Agathos, 2002; Xiao et al., 1999). It is believed that microcarriers with a high specific surface area can provide a large number of anchoring sites for the cells, which is crucial to achieve high density cell culture (Yanagi, Miyoshi, Fukuda, & Ohshima, 1992). It was indeed suggested that large pores and a high pore interconnectivity within engineered scaffolds promote oxygen/nutrients diffusion, facilitating the in-growth and distribution of cells throughout the constructs (Chiu et al., 2011; Huang et al., 2012). The CSM possess a high water absorption capacity of as much as 2300%, enabling the microcarriers to form stable suspensions in the cell culture medium.

Elasticity is one of the most important characteristics of cell microcarriers. On the one hand, it can influence cell behaviors such as differentiation and messenger expression; on the other hand,

sufficient elasticity is required for the microcarriers to withstand shear forces in stirred bioreactors (Cha, Liechty, Khademhosseini, & Peppas, 2012; K. Li et al., 2004; Radaei, Mashayekhan, & Vakilian, 2017). The elastic modulus of the CSM measured by atomic force microscopy (AFM) in the wet state was 153 kPa (see Supplementary Information), which is slightly higher than for Cytopore microcarriers. Elastic modulus analysis for soft microspheres was also conducted by other researchers using AFM. For instance, Radaei et al. (2017) measured elastic modulus values of 34~133 kPa for gelatin/chitosan blend microspheres, depending on their composition.

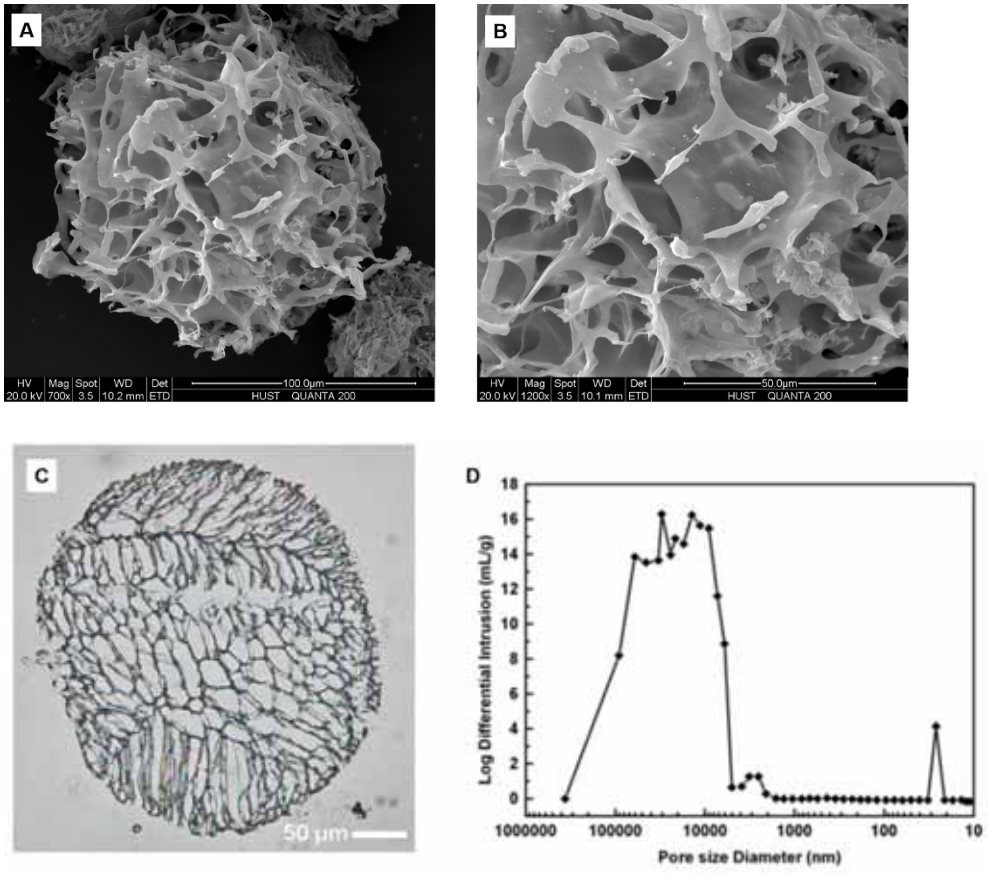

Figure 1. Structural and physical properties of the CSM: (A) SEM image; (B) Enlarged section of SEM image; (C) Optical microscopy image for a cross-section view; (D) Pore size distribution.

When the CSM are applied as microcarriers for cell culture, the highly porous structures with interconnected pores, mainly within a size range of 20~50 μm, are expected to provide a large surface area for cell attachment and a good 3D environment for cell in-growth. Their elasticity should allow them to remain intact under shear, in addition to supporting the cells. Moreover, the CSM preparation is free of toxic crosslinking agents (such as glutaraldehyde) and porogens (other than ice), making the CSM microcarriers totally toxin-free in composition, which is favorable for growth in cell cultures. Consequently, these as-prepared microcarriers were expected to have a good performance in 3D cell culture.

3.2. Cytotoxicity and blood compatibility.

The *in vitro* cytotoxicity of the CSM to L-02 cells was studied using the CCK-8 assay, and the results obtained are provided in Figure 2. The viability of L-02 cells incubated with CSM extract (non-contact; Figure 2A) and CSM suspensions (contact; Figure 2B) displayed no significant change at all the concentrations tested, with cell viability over 100% in all cases. Moreover, it is noted that the viability of L-02 cells incubated with the CSM was higher than for cells incubated with the CSM extract, which suggests that the CSM provided good anchorage facilitating cell adhesion, growth and proliferation. The blood compatibility of the CSM was evaluated by the hemolysis test (Figure 2C). It can be seen that the hemolysis rate with CSM at different concentrations (0.5, 1 and 2 mg/mL) was ca. 0.14%, 0.70% and 1.07%, respectively. According to standard ASTM-F/756-08 (2000), a hemolysis rate < 2% is defined as non-hemolytic (Seyfert, Biehl, & Schenk, 2002). The CSM are therefore considered non-hemolytic over the concentration range investigated. The trend of increasing hemolysis rate with CSM concentration is ascribed to the positive surface charges on the CSM, which could interact

electrostatically with the red blood cells. These superior cell and blood compatibility results indicate that the CSM are highly biocompatible and suitable for biomedical applications involving cell and blood contact.

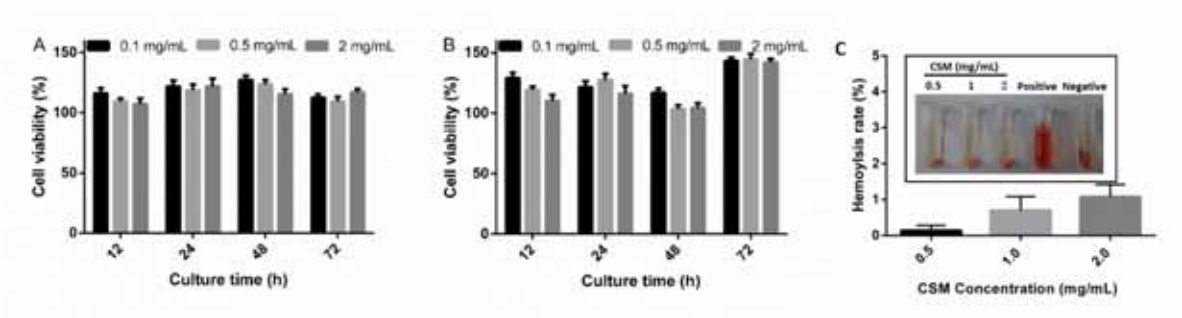

Figure 2. Biocompatibility evaluation: (A) Non-contact and (B) contact cytotoxicity of the CSM by CCK-8 assay with L-02 cells; (C) Hemolysis test for the CSM at different concentrations.

3.3. Hepatocyte culture with the CSM microcarriers and evaluation.

SEM images for L-02 cells incubated with the CSM microcarriers for 10 h are shown in Figures 3A~C. It is clear that the L-02 cells (indicated by the red arrows) were attached and grew within the internal pores of the microcarriers, in addition to the outermost surface and the external pore surface (Figure 3A). Multidirectional cell–cell interactions were established and extracellular matrix seems to be visible surrounding the cells (Figures 3B, C), suggesting that the cells adapted rapidly to the new environment in the CSM microcarriers and remained in good condition. The fractured surface of a CSM seeded with L-02 cells and incubated for 10 h was also imaged by SEM; it is presented in the Supplementary Information (Figure S2). It is clearly seen that cells are distributed across the whole fractured surface of the CSM, in addition to the edge. This indicates that cells were able to grow within the internal pores of the CSM, in addition to their external surface. To further confirm cell in-growth within the microcarriers, cell cultures

with the microcarriers were investigated by confocal microscopy after incubation for 48 h. As shown in Figures 3D~F, Calcein-AM labeled cells (green) were detected at different depths within the microcarrier from 25 μm to 75 μm. This indicates without any doubt that the cells were able to infiltrate and grow within the inner pores of the CSM.

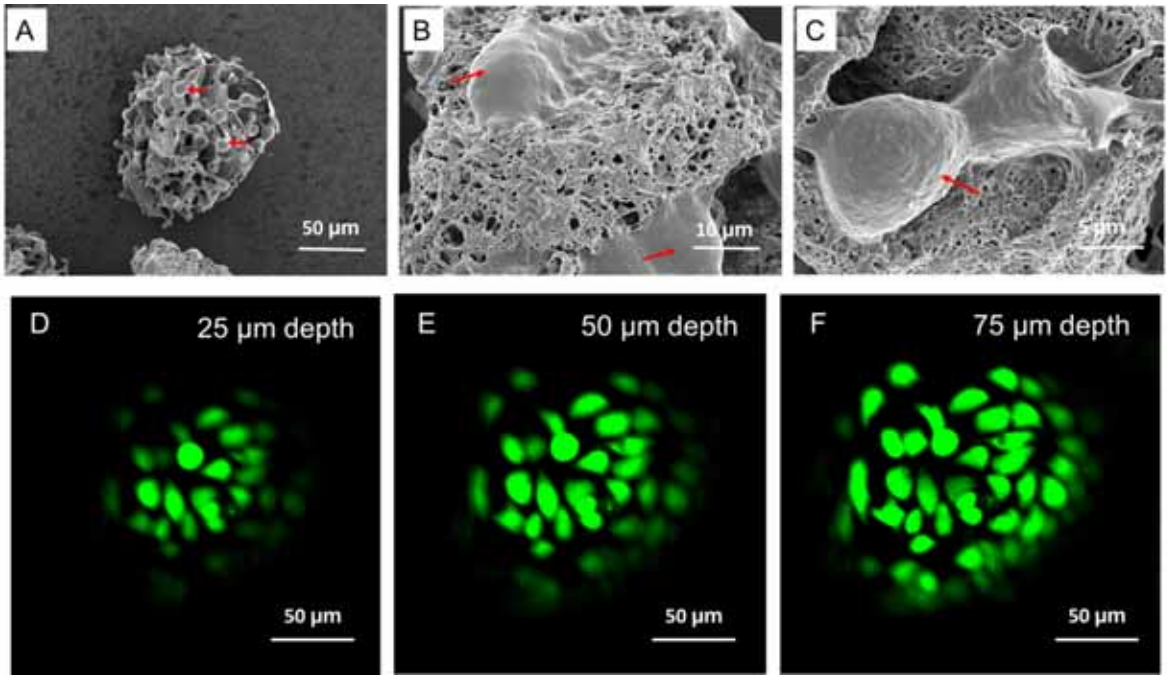

Figure 3. Hepatocyte culture with the CSM microcarriers: A~C. SEM images confirming the attachment and growth of L-02 cells on/in the CSM microcarriers after incubation for 10 h. The red arrows indicate L-02 cells; D~F. Confocal microscopic images showing cell infiltration and growth at depths of 25, 50, and 75 μm within the microcarriers after incubation for 48 h.

To evaluate cell activity, the Live/Dead assay was used to monitor the growth and proliferation of L-02 cells on/in the CSM microcarriers. Confocal laser scanning microscopy images for L-02 cells with specific live-dead staining after 12, 24, 48 or 72 h of incubation with the microcarriers are provided in Figure 4. The live cells were stained with Calcein-AM (green), while the dead cells were stained with Propidium Iodide (PI) (red). It can be seen that the cells incubated with

the microcarriers were highly active, with dead cells hardly observed over the time interval studied. The cell number in the microcarriers increased with time from 12 to 72 h, as reflected in the increased green fluorescence. These results clearly indicate that the CSM microcarriers can support cell survival and proliferation. To further examine cell activity, the cell shape was determined after incubation with the CSM for 48 h, by staining the cell nuclei and membranes with Hoechst 33258 and DiI, respectively. As shown in Figure 5, the L-02 cells exhibited an epithelial-like morphology, which implies the cells had good growth and proliferation status (Hu et al., 2013).

The success of the 3D cell culture achieved with the CSM microcarriers is attributed to their unique porous structure, with interconnected pores of 20~50 μm, in addition to the good biocompatibility of chitosan, both of which promote good cell adhesion, growth and multidirectional cell–cell interactions. It was indeed suggested that a porous structure plays a vital role in cell culture, because it promotes not only the adhesion, migration and distribution of cells, but also for the exchange of nutrients and metabolic waste (Choi, Xie, & Xia, 2009). To achieve high-performance cell culture with porous microcarriers or scaffolds, the pore size should fall within an appropriate range (Murphy, Haugh, & O'Brien, 2010; O'Brien, Harley, Yannas, & Gibson, 2005; Yannas, Lee, Orgill, Skrabut, & Murphy, 1989). If the pore size is too small, cell migration is limited, resulting in the formation of a cellular capsule around the microcarriers. Conversely, if the pore size is too large, there is a decrease in surface area limiting cell adhesion (Murphy et al., 2010). The optimal pore size can vary from tens to hundreds of microns for different cell lines, however (O'Brien et al., 2005; Yannas et al., 1989). The pores should also be interconnected to allow sufficient multidirectional cell–cell interactions within the microcarriers.

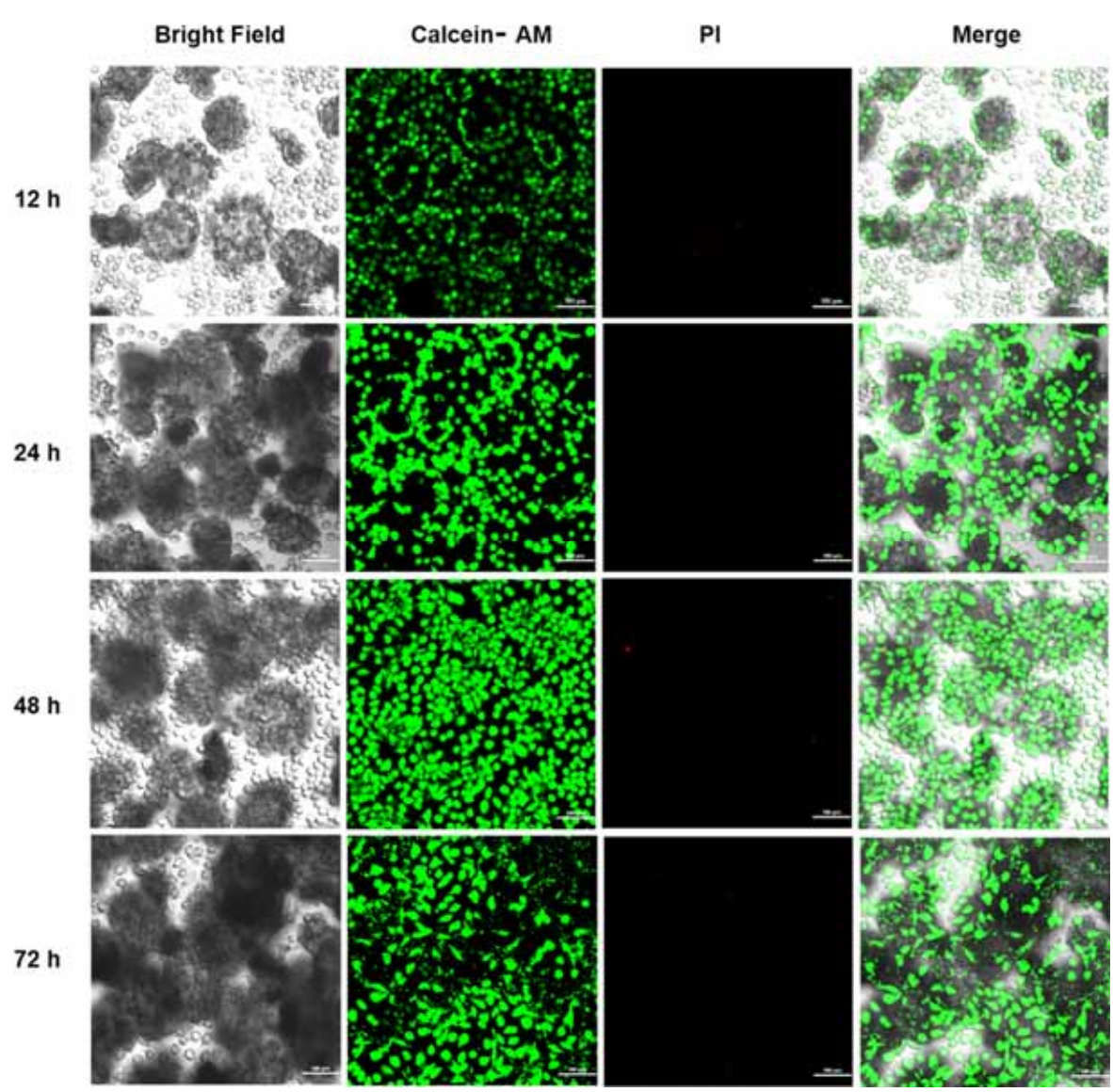

Figure 4. Confocal laser scanning microscopy images for L-02 cells after 12, 24, 48 and 72 h of incubation with the CSM microcarriers. Scale bar: 100 μm.

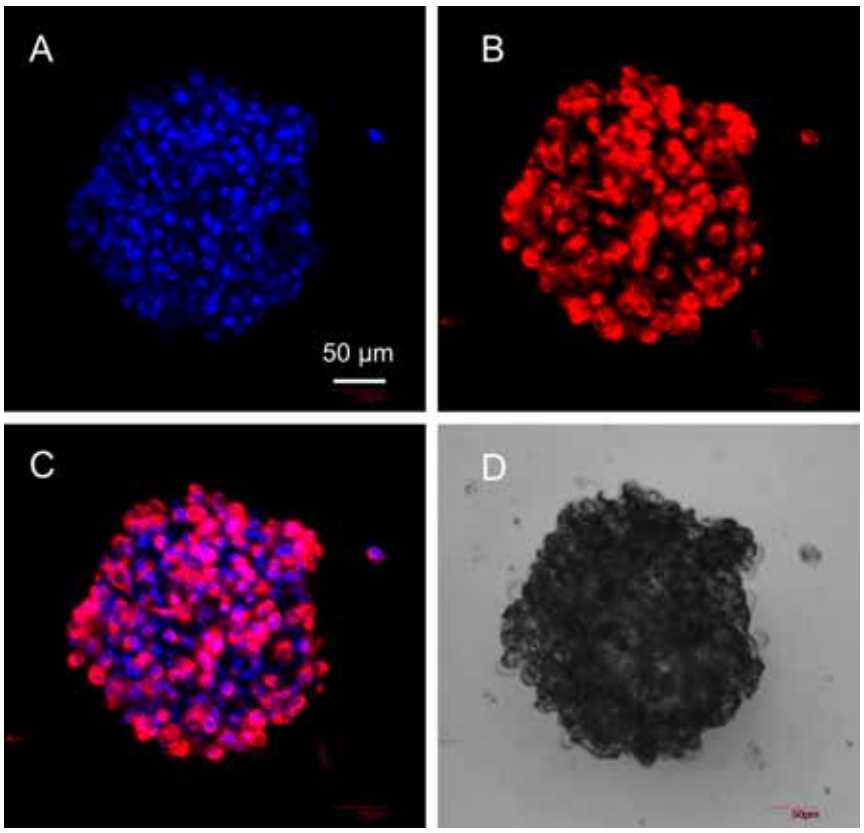

Figure 5. Cellular morphology observation by confocal microscopy after incubation with the CSM microcarriers for 48 h: A. Cell nuclei stained with Hoechst 33258; B. Cell membranes stained with DiI; C. Merged image of A and B; D. Bright field image. Scale bar: 50 μm.

3.4 Liver function investigation.

The mRNA expression of liver function-related genes including CYP2E1 (cytochromeP450, family2, subfamilyE, polypeptide1), GST (glutathione-S-transferase), MRP (multidrug resistance-related proteins) and ASS1 (argininosuccinate synthase 1) was investigated in L-02 cells cultured with the CSM microcarriers for 48 h. As can be seen in Figure 6A, the mRNA expression levels for the above genes in the CSM-cultured L-02 cells were not significantly different from L-02 cells not exposed to the microcarriers. This indicates that the

CSM microcarriers had no negative effects on the expression of liver function-related genes in the L-02 cells.

The expression of proteins related to liver functions in L-02 cells cultured on the CSM microcarriers was studied by proteomics analysis. The relative quantitative expression of the liver function-related proteins OGT1 (UDP glucuronosyl transferase), GST, HGS (hepatocyte growth factor-regulated tyrosine kinase substrate), DHE3 (glutamate dehydrogenase 1, mitochondrial), GPX 1,4 (glutathione peroxidase 1,4) and GSH0 (glutamate-cysteine ligase regulatory subunit 0) is depicted in Figure 6B. The results of western blot analysis for MRP and ASS1 are shown in the upper part of Figure 6B. Similarly to gene expression, protein expression related to liver functions in L-02 cells cultured on the CSM microcarriers was almost the same as for L-02 cells not exposed to the microcarriers. This indicates that the CSM microcarriers had no negative effects on the expression of liver function-related proteins in the L-02 cells.

To further examine the hepatocellular functions, the albumin secretion and urea synthesis ability were investigated in L-02 cells cultured on the CSM microcarriers. The results, shown in Figure 6C,D, demonstrate that as compared with cells cultured in plates, cells seeded on the CSM produced significantly more albumin each day over the 4-day period investigated, while urea synthesis was also significantly enhanced over the first two days. These results suggest that L-02 cells cultured on the CSM microcarriers had a higher activity than cells cultured in plates, which is probably due to the formation of cell-cell interactions in 3D space in the former case. With regards to the expression of the different hepatocyte functions, it is known that the establishment of adequate intracellular communication between cells is important (Nakazawa, Izumi, & Mori, 2009); because the L-02 cells cultured on the CSM microcarriers presumably had better intercellular communication than in the cell monolayers, they may be able to express

437 higher hepatocyte functions. It is noted that the secretion of albumin and the synthesis of urea
438 decreased over time for cells cultured on both the microcarriers and in plates (Figure 6C,D).
439 Similar results for hepatocyte functions *in vitro* were reported in the literature (Chua et al., 2005;
440 Seo et al., 2005). For example, Chua et al. (2005) reported hepatocyte culture on galactosylated
441 poly(ε-caprolactone-*co*-ethyl ethylene phosphate) nanofiber and film scaffolds. They also found
442 that the albumin and urea synthesis functions of the hepatocytes decreased over a 5-day period.
443 However, other studies demonstrated that the hepatocyte functions were maintained or even
444 increased over time (Isoda et al., 2004). This shows the complexity of hepatocyte function
445 maintenance, in that the expression of hepatocyte functions could be influenced by different
446 biochemical and topological cues, among others.

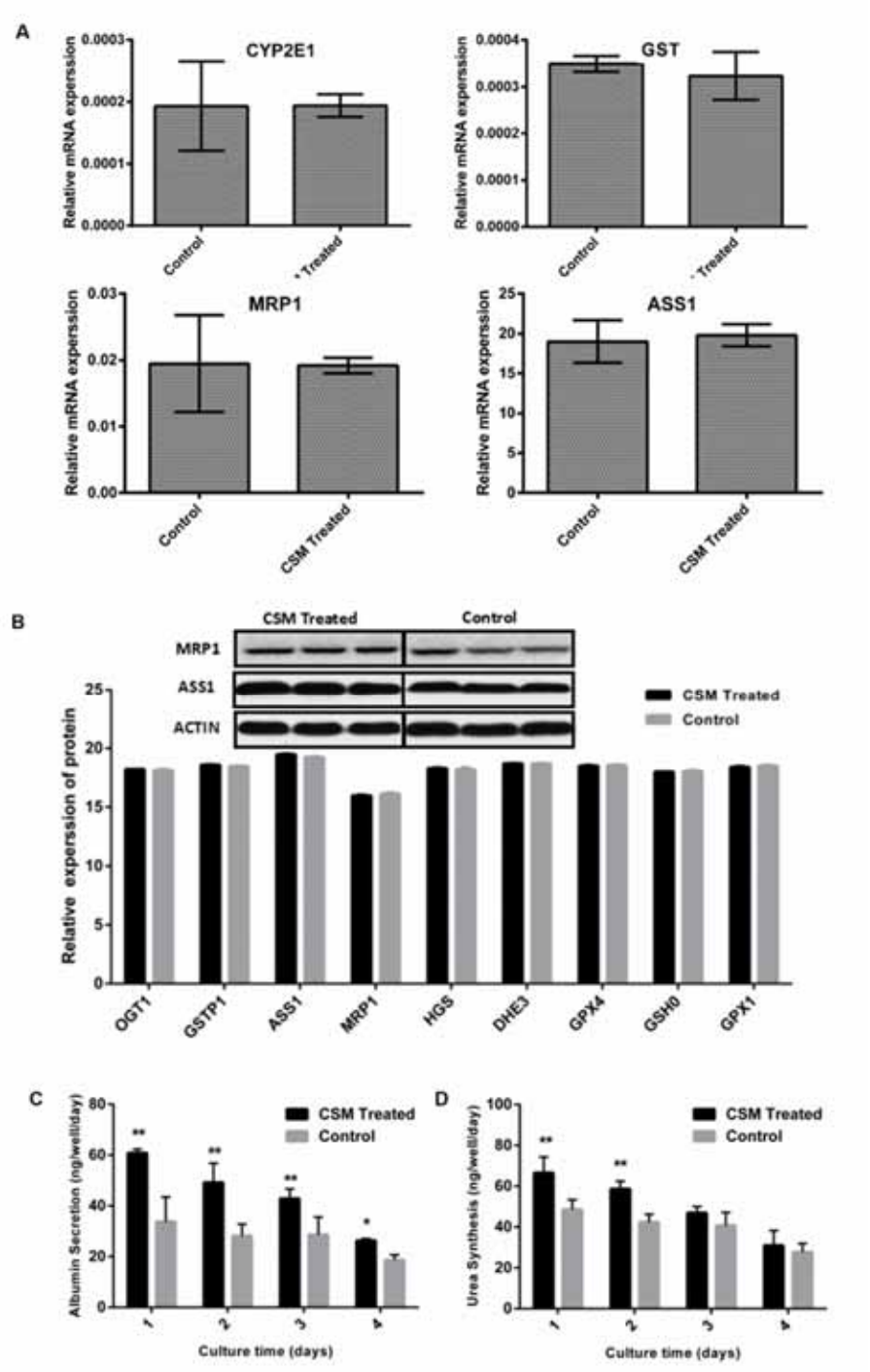

447

448 Figure 6. Liver function evaluation for L-02 cells cultured with the CSM microcarriers: (A)
449 mRNA expression of liver function-related genes; (B) Liver function-related protein expression;
450 (C) Albumin secretion; (D) Urea synthesis.

4. CONCLUSIONS

Microcarriers based on porous chitosan microspheres (CSM) appropriate for 3D cell culture were developed, by adapting a simple emulsion-based thermally induced phase separation (TIPS) process to produce interconnected pores with a size appropriate to accommodate the cells. The mild preparation conditions used for the CSM, free of toxic reagents, ensured superior biocompatibility of the carriers. 3D cell culture was achieved using these microcarriers with hepatocytes, as cell growth was allowed within the internal pores, in addition to the outermost surface and the external pore surface, and multidirectional cell–cell interactions were observed. These CSM microcarriers are favorable to maintain the activity and functions of the cells in comparison with 2D cell culture in plates. On the basis of the results obtained, it is believed that these CSM microcarriers have great potential as efficient platforms for 3D cell culture.

ACKNOWLEDGMENT

The authors acknowledge the National Natural Science Foundation of China (General Program, Nos. 21574050 and 21774039), China Postdoctoral Science Foundation (General Program, No. 2015M580640), Science and Technology Support Plan in Jiangsu Province, China (BE2014684) and the independent innovation research funding of Huazhong University of Science and Technology (2014XJGH009) for their financial support.

SUPPLEMENTARY INFORMATION

Supplementary information associated with this article can be found in the online version. The following files are available free of charge: Protocols for the determination of the porosity, density, pore size distribution, water absorption, elastic modulus, and the biocompatibility studies of the CSM, SEM image of a fracture surface of the CSM seeded with L-02 cells (DOCX).

REFERENCES

Achilli, T.-M., Meyer, J., & Morgan, J. R. (2012). Advances in the formation, use and understanding of multi-cellular spheroids. *Expert Opinion on Biological Therapy,* 12(10), 1347-1360.

Ahmadi, R., Mordan, N., Forbes, A., & Day, R. M. (2011). Enhanced attachment, growth and migration of smooth muscle cells on microcarriers produced using thermally induced phase separation. *Acta Biomaterialia,* 7(4), 1542-1549.

Anitha, A., Sowmya, S., Kumar, P. S., Deepthi, S., Chennazhi, K. P., Ehrlich, H., ... & Jayakumar, R. (2014). Chitin and chitosan in selected biomedical applications. *Progress in Polymer Science*, 39(9), 1644-1667.

Asghar, W., El Assal, R., Shafiee, H., Pitteri, S., Paulmurugan, R., & Demirci, U. (2015). Engineering cancer microenvironments for in vitro 3-D tumor models. *Materials Today,* 18(10), 539-553.

Cha, C., Liechty, W. B., Khademhosseini, A., & Peppas, N. A. (2012). Designing biomaterials to direct stem cell fate. *ACS Nano,* 6(11), 9353-9358.

Chen, A. K.-L., Reuveny, S., & Oh, S. K. W. (2013). Application of human mesenchymal and pluripotent stem cell microcarrier cultures in cellular therapy: Achievements and future direction. *Biotechnology Advances,* 31(7), 1032-1046.

Chiu, Y.-C., Cheng, M.-H., Engel, H., Kao, S.-W., Larson, J. C., Gupta, S., & Brey, E. M. (2011). The role of pore size on vascularization and tissue remodeling in PEG hydrogels. *Biomaterials,* 32(26), 6045-6051.

Choi, S. W., Xie, J., & Xia, Y. (2009). Chitosan - based inverse opals: Three - dimensional scaffolds with uniform pore structures for cell culture. *Advanced Materials,* 21(29), 2997-3001.

Chua, K.-N., Lim, W.-S., Zhang, P., Lu, H., Wen, J., Ramakrishna, S., . . . Mao, H.-Q. (2005). Stable immobilization of rat hepatocyte spheroids on galactosylated nanofiber scaffold. *Biomaterials,* 26(15), 2537-2547.

506 Chung, H. J., Kim, I. K., Kim, T. G., & Park, T. G. (2008). Highly open porous biodegradable
507 microcarriers: in vitro cultivation of chondrocytes for injectable delivery. *Tissue*
508 *Engineering Part A*, 14(5), 607-615.
509 Costa, C. N., Teixeira, V. G., Delpech, M. C., Souza, J. V. S., & Costa, M. A. S. (2015).
510 Viscometric study of chitosan solutions in acetic acid/sodium acetate and acetic
511 acid/sodium chloride. *Carbohydrate Polymers,* 133, 245-250.
512 Custódio, C. A., Cerqueira, M. T., Marques, A. P., Reis, R. L., & Mano, J. F. (2015). Cell
513 selective chitosan microparticles as injectable cell carriers for tissue regeneration.
514 *Biomaterials*, 43, 23-31.
515 Duan, B., Zheng, X., Xia, Z., Fan, X., Guo, L., Liu, J., . . . Zhang, L. (2015). Highly
516 biocompatible nanofibrous microspheres self-assembled from chitin in NaOH/urea
517 aqueous solution as cell carriers. *Angewandte Chemie International Edition,* 54(17),
518 5152-5156.
519 Fang, J., Zhang, Y., Yan, S., Liu, Z., He, S., Cui, L., & Yin, J. (2014). Poly(l-glutamic
520 acid)/chitosan polyelectrolyte complex porous microspheres as cell microcarriers for
521 cartilage regeneration. *Acta Biomaterialia,* 10(1), 276-288.
522 Griffith, C. K., Miller, C., Sainson, R. C. A., Calvert, J. W., Jeon, N. L., Hughes, C. C. W., &
523 George, S. C. (2005). Diffusion limits of an in vitro thick prevascularized tissue. *Tissue*
524 *Engineering,* 11(1-2), 257-266.
525 Healthcare, G., & Biosciences, A. (2005). *Microcarrier Cell Culture: Principles and Methods*:
526 GE Healthcare/Amersham Biosciences.
527 Higuchi, A., Ling, Q.-D., Kumar, S. S., Munusamy, M., Alarfajj, A. A., Umezawa, A., & Wu,
528 G.-J. (2014). Design of polymeric materials for culturing human pluripotent stem cells:
529 Progress toward feeder-free and xeno-free culturing. *Progress in Polymer Science,* 39(7),
530 1348-1374.
531 Hollister, S. J. (2005). Porous scaffold design for tissue engineering. *Nature Materials,* 4, 518.
532 Huang, C.-C., Wei, H.-J., Yeh, Y.-C., Wang, J.-J., Lin, W.-W., Lee, T.-Y., . . . Sung, H.-W.
533 (2012). Injectable PLGA porous beads cellularized by hAFSCs for cellular
534 cardiomyoplasty. *Biomaterials,* 33(16), 4069-4077.
535 Hu, X., Yang, T., Li, C., Zhang, L., Li, M., Huang, W., & Zhou, P. (2013). Human fetal
536 hepatocyte line, L-02, exhibits good liver function in vitro and in an acute liver failure
537 model. *Transplantation proceedings*, 45(2), 695-700.
538 Ikonomou, L., Drugmand, J. C., Bastin, G., Schneider, Y. J., & Agathos, S. N. (2002).
539 Microcarrier culture of lepidopteran cell lines: Implications for growth and recombinant
540 protein production. *Biotechnology Progress,* 18(6), 1345-1355.
541 Isoda, K., Kojima, M., Takeda, M., Higashiyama, S., Kawase, M., & Yagi, K. (2004).
542 Maintenance of hepatocyte functions by coculture with bone marrow stromal cells.
543 *Journal of Bioscience and Bioengineering,* 97(5), 343-346.
544 Kehr, N. S. (2016). Enantiomorphous periodic mesoporous organosilica-based nanocomposite
545 hydrogel scaffolds for cell adhesion and cell enrichment. *Biomacromolecules*, 17(3),
546 1117-1122.
547 Lee, G. Y., Kenny, P. A., Lee, E. H., & Bissell, M. J. (2007). Three-dimensional culture models
548 of normal and malignant breast epithelial cells. *Nature Methods,* 4, 359.
549 Li, J., Wu, X., Wu, Y., Tang, Z., Sun, X., Pan, M., . . . Liu, H. (2017). Porous chitosan
550 microspheres for application as quick in vitro and in vivo hemostat. *Materials Science*
551 *and Engineering: C,* 77, 411-419.

Li, K., Wang, Y., Miao, Z., Xu, D., Tang, Y., & Feng, M. (2004). Chitosan/gelatin composite microcarrier for hepatocyte culture. *Biotechnology Letters,* 26(11), 879-883.

Mazza, G., Rombouts, K., Rennie Hall, A., Urbani, L., Vinh Luong, T., Al-Akkad, W., . . . Pinzani, M. (2015). Decellularized human liver as a natural 3D-scaffold for liver bioengineering and transplantation. *Scientific Reports,* 5, 13079.

Motealleh, A., Hermes, H., Jose, J., & Kehr, N. S. (2018). Chirality-dependent cell adhesion and enrichment in Janus nanocomposite hydrogels. *Nanomedicine: Nanotechnology, Biology and Medicine*, 14(2), 247-256.

Motealleh, A., & Kehr, N. S. (2017). Janus nanocomposite hydrogels for chirality-dependent cell adhesion and migration. *ACS applied materials & interfaces*, 9(39), 33674-33682.

Murphy, C. M., Haugh, M. G., & O'Brien, F. J. (2010). The effect of mean pore size on cell attachment, proliferation and migration in collagen–glycosaminoglycan scaffolds for bone tissue engineering. *Biomaterials,* 31(3), 461-466.

Nakazawa, K., Izumi, Y., & Mori, R. (2009). Morphological and functional studies of rat hepatocytes on a hydrophobic or hydrophilic polydimethylsiloxane surface. *Acta Biomaterialia,* 5(2), 613-620.

Nina, P., Raheleh, A., & M., D. R. (2015). A novel method for differentiation of human mesenchymal stem cells into smooth muscle-like cells on clinically deliverable thermally induced phase separation microspheres. *Tissue Engineering Part C: Methods,* 21(4), 404-412.

O'Brien, F. J., Harley, B. A., Yannas, I. V., & Gibson, L. J. (2005). The effect of pore size on cell adhesion in collagen-GAG scaffolds. *Biomaterials,* 26(4), 433-441.

Pampaloni, F., Reynaud, E. G., & Stelzer, E. H. K. (2007). The third dimension bridges the gap between cell culture and live tissue. *Nature Reviews Molecular Cell Biology,* 8, 839.

Pellá, M. G., Lima-Tenório, M. K., Tenório-Neto, E. T., Guilherme, M. R., Muniz, E. C., & Rubira, A. F. (2018). Chitosan-based hydrogels: From preparation to biomedical applications. *Carbohydrate polymers*, 196, 233-245.

Radaei, P., Mashayekhan, S., & Vakilian, S. (2017). Modeling and optimization of gelatin-chitosan micro-carriers preparation for soft tissue engineering: Using response surface methodology. *Materials Science and Engineering: C,* 75, 545-553.

Seo, S.-J., Akaike, T., Choi, Y.-J., Shirakawa, M., Kang, I.-K., & Cho, C.-S. (2005). Alginate microcapsules prepared with xyloglucan as a synthetic extracellular matrix for hepatocyte attachment. *Biomaterials,* 26(17), 3607-3615.

Seyfert, U. T., Biehl, V., & Schenk, J. (2002). In vitro hemocompatibility testing of biomaterials according to the ISO 10993-4. *Biomolecular Engineering,* 19(2), 91-96.

Song, J., Chen, C., Wang, C., Kuang, Y., Li, Y., Jiang, F., . . . Hu, L. (2017). Superflexible wood. *ACS Applied Materials & Interfaces,* 9(28), 23520-23527.

Tedesco, M. T., Di Lisa, D., Massobrio, P., Colistra, N., Pesce, M., Catelani, T., ... & Pastorino, L. (2018). Soft chitosan microbeads scaffold for 3D functional neuronal networks. *Biomaterials*, 156, 159-171.

Tripathi, A., & Melo, J. S. (2015). Preparation of a sponge-like biocomposite agarose-chitosan scaffold with primary hepatocytes for establishing an in vitro 3D liver tissue model. *RSC Advances,* 5(39), 30701-30710.

Van Wezel, A. L. (1967). Growth of cell-strains and primary cells on micro-carriers in homogeneous culture. *Nature,* 216, 64.

Westin, C. B., Trinca, R. B., Zuliani, C., Coimbra, I. B., & Moraes, Â. M. (2017). Differentiation of dental pulp stem cells into chondrocytes upon culture on porous chitosan-xanthan scaffolds in the presence of kartogenin. *Materials Science and Engineering: C*, 80, 594-602.

Wu, X. B., Peng, C. H., Huang, F., Kuang, J., Yu, S. L., Dong, Y. D., & Han, B. S. (2011). Preparation and characterization of chitosan porous microcarriers for hepatocyte culture. *Hepatobiliary & Pancreatic Diseases International*, 10(5), 509-515.

Xiao, C., Huang, Z., Li, W., Hu, X., Qu, W., Gao, L., & Liu, G. (1999). High density and scale-up cultivation of recombinant CHO cell line and hybridomas with porous microcarrier Cytopore. *Cytotechnology,* 30(1), 143-147.

Yan, S., Xia, P., Xu, S., Zhang, K., Li, G., Cui, L., & Yin, J. (2018). Nanocomposite porous microcarriers based on strontium-substituted HA-g-poly (γ-benzyl-l-glutamate) for bone tissue engineering. *ACS applied materials & interfaces*, 10(19), 16270-16281.

Yanagi, K., Miyoshi, H., Fukuda, H., & Ohshima, N. (1992). A packed-bed reactor utilizing porous resin enables high density culture of hepatocytes. *Applied Microbiology and Biotechnology,* 37(3), 316-320.

Yannas, I. V., Lee, E., Orgill, D. P., Skrabut, E. M., & Murphy, G. F. (1989). Synthesis and characterization of a model extracellular matrix that induces partial regeneration of adult mammalian skin. *Proceedings of the National Academy of Sciences,* 86(3), 933-937.

Yu, C., Kornmuller, A., Brown, C., Hoare, T., & Flynn, L. E. (2017). Decellularized adipose tissue microcarriers as a dynamic culture platform for human adipose-derived stem/stromal cell expansion. *Biomaterials,* 120, 66-80.

Zhang, S., Ma, B., Wang, S., Duan, J., Qiu, J., Li, D., ... & Liu, H. (2018). Mass-production of fluorescent chitosan/graphene oxide hybrid microspheres for in vitro 3D expansion of human umbilical cord mesenchymal stem cells. *Chemical Engineering Journal*, 331, 675-684.

Zhang, Z., & Ma, P. X. (2015). From nanofibrous hollow microspheres to nanofibrous hollow discs and nanofibrous shells. *Macromolecular Rapid Communications,* 36(19), 1735-1741.

Supplementary Information

Porous Chitosan Microspheres as Microcarriers for 3D Cell Culture

Lixia Huang,[1‡] *Lin Xiao,*[1‡] *Abishek Jung Poudel,*[1] *Jixiang Li,*[2] *Ping Zhou,*[3] *Mario Gauthier,*[4] *Haiqing Liu,*[2*] *Zhihong Wu,*[5*] *Guang Yang*[1*]

[1] Department of Biomedical Engineering, College of Life Science and Technology, Huazhong University of Science and Technology, 1037 Luoyu Road, Wuhan 430074, China.

[2] Fujian Provincial Key Laboratory of Polymer Materials, College of Material Science and Engineering, Fujian Normal University, 8 Shangsan Road, Fuzhou 350007, China.

[3] Institute of Organ Transplantation, Tongji Medical School, Huazhong University of Science and Technology, 13 Hangkong Road, Wuhan 430074, China.

[4] Department of Chemistry, University of Waterloo, 200 University Avenue West, Waterloo N2L 3G1, Canada.

[5] Department of Orthopaedic Surgery, Peking Union Medical College Hospital, Peking Union Medical College, 1 Shuaifuyuan Road, Beijing 100730, China.

Corresponding Authors

*E-mail: yang_sunny@yahoo.com. Tel: +86 27-87793523. Fax: +86 27-87792265.

*E-mail: haiqing.liu@gmail.com. Tel: +86 591-83404938. Fax: +86 591-83404938.

*E-mail: wuzh3000@126.com. Tel: +86 10-69154259. Fax: +86 10-69154259.

‡These authors contributed equally.

Porosity and density

The porosity of the CSM was determined *via* a liquid displacement method with ethanol as the displacement liquid, as reported in previous studies (Guan, Fujimoto, Sacks, & Wagner, 2005; Li et al., 2017). Briefly, a certain amount of CSM (M_S) was added to a pycnometer containing absolute ethanol (M_1). Then the bottle was subjected to low vacuum until the air in the scaffold was completely removed and replaced with ethanol. The bottle was then completely filled with ethanol and was weighed as M_2. Then the CSM saturated with ethanol were collected by carefully draining the ethanol, the remaining ethanol on the CSM surface was removed with filter paper. The pycnometer containing wet CSM was weighed as M_3. The volume of the CSM was calculated as $V_S = (M_1 - M_2 + M_3 - M) / \rho$ (ethanol). The density (ρ) and porosity (P) were calculated using Equations (S1) and (S2):

$$\rho = M_S \rho(\text{ethanol}) / (M_1 + M_3 - M - M_2) \quad (S1)$$

$$P = V_P/V_S = [(M_3 - M - M_S) / (M_1 - M_2 + M_3 - M)] \times 100\% \quad (S2)$$

Pore size distribution

The pore size distribution was estimated with a mercury injection apparatus (AutoPore IV 9500, Micromeritics Instrument Corporation). The equipment operated at pressures of 10 kPa to 300 MPa, to probe pores with diameters ranging from 150 μm to 0.005 μm. The CSM samples were dried with silica gel prior to the measurements.

Water absorption capacity

The water absorption capacity of the CSM was investigated as described previously [S1]. A certain amount of dry CSM (M_d) was immersed into phosphate-buffered saline (PBS, pH 7.4) solution. The glass beaker containing the mixture was evacuated for 3 min, to allow filling of the pores in the CSM by the solution, and allowed to stand for 24 h. Subsequently, the PBS solution was discarded and excess liquid was removed with filter paper. The mass of the wet CSM (M_w) was measured. Triplicate measurements were made for each sample. The water absorption ratio (A) was calculated using Equation (S3):

$$A = [(M_w - M_d)/ M_d] \times 100\% \quad (S3)$$

Elastic modulus

The dry CSM were put into PBS solution and stirred at 400 rpm for 30 min. The elastic modulus (E) of the wet CSM was determined by analysis of the force-displacement curve on an atomic force microscopy (AFM) apparatus. The plot of force versus distance between the probe and the CSM surface was recorded as shown below (Figure S1). The set point was selected as 14 nN for a quadratic pyramid tip and the cantilever was lowered at a velocity of 1 μm/s. The constant spring of the cantilever (Kc) was 0.68 N/m. The local elastic modulus of the sample was calculated using the equations below (Kuznetsova, Starodubtseva, Yegorenkov, Chizhik, & Zhdanov, 2007; Radaei, Mashayekhan, & Vakilian, 2017; Hertz, 1881).

$$E = \frac{F}{\pi a^2} \qquad \text{(S4)}$$

$$F = Kc \times Ks \times \Delta V, \text{ in which } Ks = \Delta Z1/\Delta V1 \qquad \text{(S5)}$$

$$a = \sqrt[3]{\frac{3FR}{4E}} \qquad \text{(S6)}$$

In these equations, E is elastic modulus of the CSM; F is the force applied; a is the Hertzian contact radius; Kc is the constant spring of cantilever (in this study, it was 0.68N/m.); Ks is the displacement sensitivity, which is the displacement of the scanner when the operating point changes by one volt. R is the radius of the CSM tested. Since the values of ΔV, ΔV_1, ΔZ_1 are known for the force curve (Figure S1), the elastic modulus (E) of the CSM can be calculated as 153 kPa.

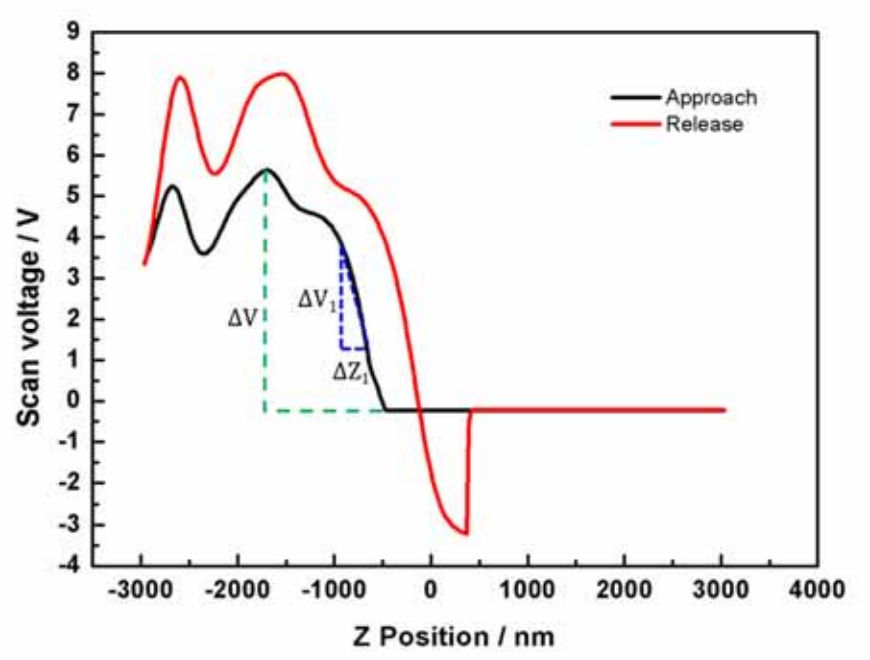

Figure S1. Analysis of the AFM force curve.

Biocompatibility assay

Cytotoxicity assay. For the non-contact cytotoxicity assays, a CSM extract was prepared according to ISO 10993-5. Briefly, sterilized CSM were immersed in cell culture medium at different concentrations of 0.5, 1.0 and 2.0 mg/mL at 37℃ for 72 h. Solid components were then removed by centrifugation at 10000 rpm for 5 min. The collected supernatant was used as CSM extract after filtration through a 0.22 μm filter membrane. The L-02 cells were seeded at 1×10^4 cells/well in a 96-well plate and incubated at 37 ℃ in a 5% CO_2 atmosphere overnight. The medium was then replaced with the CSM extract, using the cell culture medium as control. After incubation for 12, 24, 48 or 72 h, the cells were treated with 10 μL/well of CCK-8 (Dojindo, Japan) solution with shaking for 5 min and incubated for another 30 min. Absorbance values were measured in triplicate at 450 nm using a microplate reader (Multiskan GO, Thermo Fisher, USA). For contact cytotoxicity, the cells were seeded with the CSM at concentrations of 0.5, 1.0 and 2.0 mg/mL, and the above procedures for the assessment of non-contact cytotoxicity were followed. Cell viability was calculated using Equation (S7), where OD_S, OD_B and OD_N are the OD values for the sample, the blank control and the negative control, respectively.

$$\text{Cell viability} = \frac{OD_S - OD_B}{OD_N - OD_B} \times 100\% \qquad \text{(S7)}$$

Hemolysis rate test. To evaluate the blood compatibility of the CSM, the hemolysis rate was determined by the method described below. Fresh blood was collected from a healthy rabbit and mixed with heparin immediately to prevent clotting, before dilution with normal saline at a volume ratio of 1:1.25. The CSM samples at different concentrations (i.e. 0.5, 1.0 and 2.0 mg/mL) were

pre-swelled in normal saline overnight. Distilled water and normal saline were used as positive and negative controls, respectively. All the samples (1.5 mL) were stored at 37°C in the presence of 50 μL of diluted blood for 30 min. The samples were then centrifuged at 1000 rpm for 5 min and the supernatant was subjected to absorbance measurements at 545 nm on a microplate reader (Multiskan GO, Thermo Scientific). The hemolysis rate was calculated using Equation (S8), where OD_S, OD_N, and OD_P are the absorbance values for the sample, the negative control and the positive control, respectively.

$$\text{Hemolysis Rate} = [(OD_S - OD_N)/(OD_P - OD_N)] \times 100\% \quad \text{(S8)}$$

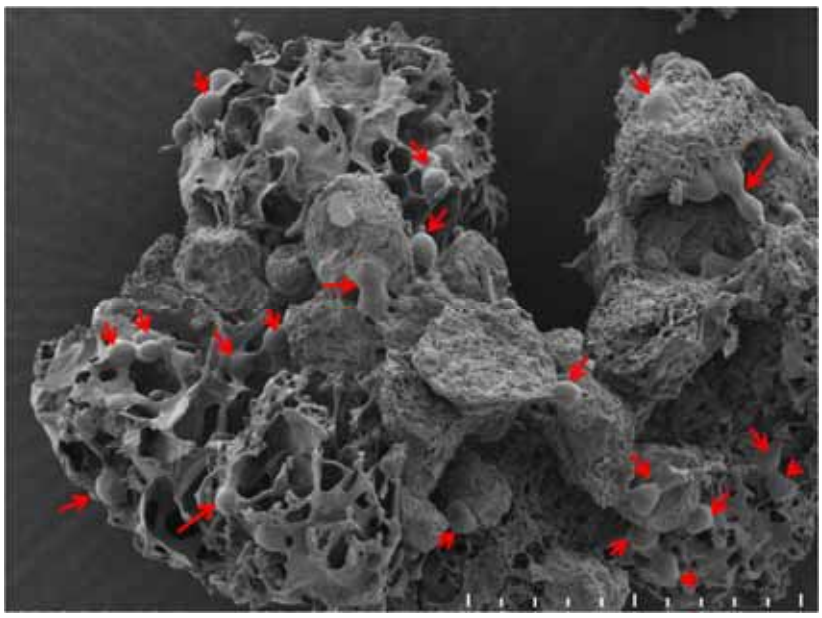

Figure S2 SEM image for a fractured surface of the CSM seeded with L-02 cells (indicated with red arrows) after 10 h of incubation. Scale bar: 100 μm.

References

Guan, J., Fujimoto, K. L., Sacks, M. S., & Wagner, W. R. (2005). Preparation and characterization of highly porous, biodegradable polyurethane scaffolds for soft tissue applications. Biomaterials, 26(18), 3961-3971.

Hertz, H. (1881). Ueber den kontakt elastischer koerper. *Journal für die reine und angewandte Mathematik*. 92, 156-171.

Kuznetsova, T. G., Starodubtseva, M. N., Yegorenkov, N. I., Chizhik, S. A., & Zhdanov, R. I. (2007). Atomic force microscopy probing of cell elasticity. *Micron,* 38(8), 824-833.

Li, J., Wu, X., Wu, Y., Tang, Z., Sun, X., Pan, M., . . . Liu, H. (2017). Porous chitosan microspheres for application as quick in vitro and in vivo hemostat. *Materials Science and Engineering: C,* 77, 411-419.

Radaei, P., Mashayekhan, S., & Vakilian, S. (2017). Modeling and optimization of gelatin-chitosan micro-carriers preparation for soft tissue engineering: Using Response Surface Methodology. *Materials Science and Engineering: C,* 75, 545-553.